HHS Public Access

Author manuscript

Int J Dev Neurosci. Author manuscript; available in PMC 2023 April 01.

Published in final edited form as:

Int J Dev Neurosci. 2022 April ; 82(2): 146–158. doi:10.1002/jdn.10167.

Structural Abnormalities in Pediatric Moyamoya Disease Revealed by Clinical Magnetic Resonance Imaging, Regionally Distributed Relative Signal Intensities and Volumes

Prahar Ijner[1], **Grace Tompkins**[2], **Tadashi Shiohama**[3], **Emi Takahashi**[4,5,6], **Jacob Levman**[1]

[1]Department of Computer Science, St. Francis Xavier University, Antigonish, NS, B2G 2W5, Canada

[2]Department of Mathematics and Statistics, St. Francis Xavier University, Antigonish, NS, B2G 2W5, Canada

[3]Department of Pediatrics, Graduate School of Medicine, Chiba University, Japan

[4]Division of Newborn Medicine, Department of Medicine, Boston Children's Hospital, 401 Park Dr., Boston, MA 02215, USA

[5]Athinoula A. Martinos Center for Biomedical Imaging, Massachusetts General Hospital, Charlestown, MA, USA

[6]Harvard Medical School, Department of Radiology, Boston, MA 02115, USA

Abstract

Moyamoya disease (MMD) is a rare, progressive cerebrovascular disorder, with an unknown etiology and pathogenesis. It is characterized by steno-occlusive changes at the terminal portion of the internal carotid artery (ICA), which is accompanied by variable development of the basal collaterals called moyamoya vessels. In this study, we investigate the potential for structural T1 magnetic resonance imaging (MRI) to help characterize MMD clinically, with the help of regionally distributed relative signal intensities (RRSIs) and volumes (RRVs). These RRSIs and RRVs provide the ability to characterize aspects of regional brain development and represent an extension to existing automated biomarker extraction technologies. This study included 269 MRI examinations from MMD patients and 993 MRI examinations from neurotypical controls, with regional biomarkers compared between groups with the area under the receiver operating characteristic curve (AUC). Results demonstrate abnormal presentation of RRSIs and RRVs in the insula (15-20 year old cohort, left AUC: 0.74, right AUC: 0.71), and the lateral orbitofrontal region (5-10 year old cohort, left AUC: 0.67; 15-20 year cohort, left AUC: 0.62, right AUC: 0.65). Results indicate that RRSIs and RRVs may help in characterizing brain development, assist in the assessment of the presentation of the brains of children with MMD, and may help overcome standardization challenges in multi-protocol clinical MRI. Further investigation of the potential

*Correspondence to: Jacob Levman, PhD, Canada Research Chair in Bioinformatics, 5005 Chapel Square, Antigonish, NS, Canada, B2G 2K9, jlevman@stfx.ca.

JL conceived the analysis; JL performed the supervision; PI, TS and GT did the manuscript authoring; GT, JL, PI, TS and ET did the manuscript editing/approval; PI performed the software development.

Additional discussion is provided in the supplementary materials.

for RRSIs and RRVs in clinical imaging is warranted and supported through the release of open source software.

Graphical Abstract

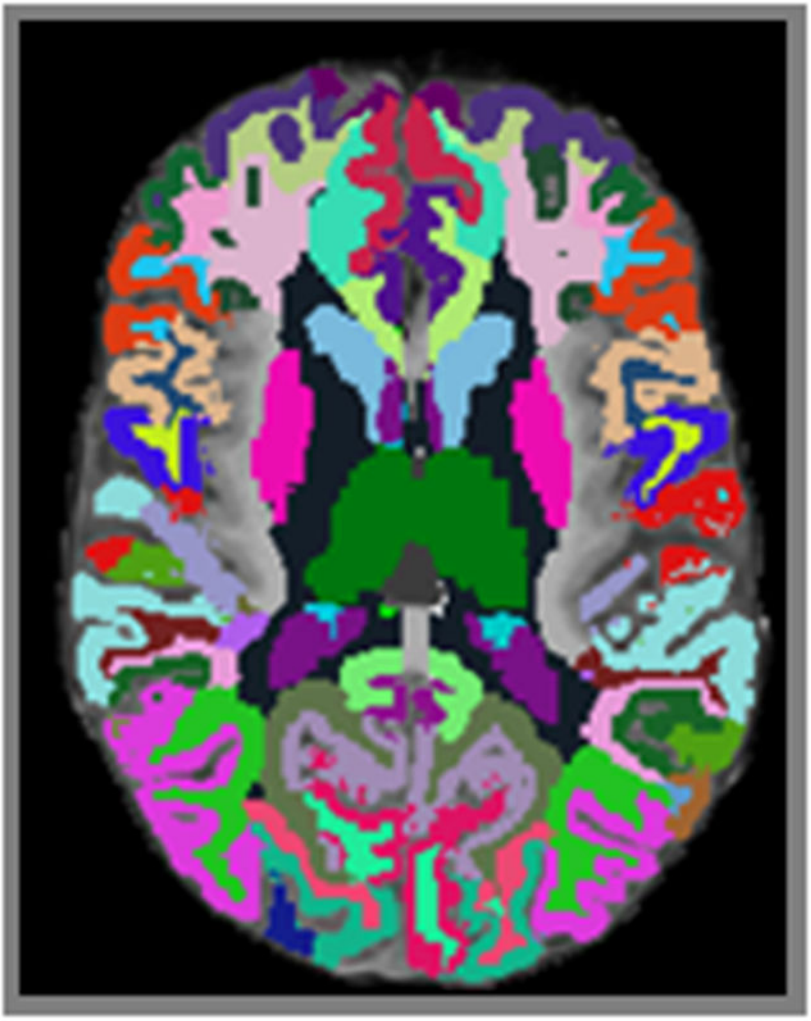

Moyamoya disease (MMD) is characterized by steno-occlusive changes at the terminal portion of the internal carotid artery, resulting in a progressive cerebrovascular disorder. In this study, we investigate the potential for regional relative volumes (RRVs) and signal intensities (RRSIs) extracted from structural magnetic resonance imaging to characterize abnormal neurodevelopment in MMD. Results demonstrate abnormal presentation of the insula, the orbitofrontal region, and the caudate. Open source software is made available to facilitate other researchers in calculating RRVs and RRSIs as part of future studies.

Introduction

Moyamoya disease (MMD) is a rare, progressive cerebrovascular disorder, with an unknown pathogenesis. Moyamoya's etiology, which remains unclear, is multifactorial, including both

genetic and environmental factors (Ganesan, 2010). Genetic factors in the etiology of MMD have been proposed for a variety of reasons, including increased prevalence in certain ethnicities (Baba et al., 2008; Ahn et al., 2014; Miao et al., 2010; Kainth et al., 2013), pedigree analysis (Mineharu et al., 2006; Chaudhuri et al., 1993), the genetic susceptibility of ring finger protein 213 (*RNF213)* gene (Kamada et al., 2011; Liu et al., 2011), the fact that approximately 1 in 10 people with MMD are closely related to someone who is also affected, and moyamoya having been identified in identical twins (Chaudhuri et al., 1993) and siblings (Papavasiliou et al., 2007). The disease also complicates several other genetic disorders such as Down's syndrome, neurofibromatosis, and tuberous sclerosis complex (Chaudhuri et al., 1993). Moyamoya was first described in 1957 when symptoms of cerebral infarction were found with hypoplasia of the internal carotid arteries in the Japanese population (Smith, 2015). The disease is named after the distinct appearance of cerebral vessels in the angiograph, which resemble a puff of smoke, or "moyamoya" in Japanese. It is characterized by steno-occlusive changes at the terminal portion of the internal carotid artery (ICA), which is accompanied by variable development of the basal collaterals called moyamoya vessels. Moyamoya vessels are formed to compensate for the reduced blood supply to the brain due to the narrowing of the ICA, however they stop working overtime. These vessels are often seen in the proximal portions of the middle and anterior cerebral arteries (Yamada, et al., 1995). Patients with MMD show different patterns of brain damage, and may experience recurrent multiple transient ischemic attacks, cerebral infarction, and intracranial bleeding (Qiao et al., 2017). Some patients manifest complex clinical behaviour including epilepsy, headaches, and a combination of motor, sensory, speech, visual, and cognitive dysfunction (Suzuki and Kodama, 1983; Duan, 2012).

Automated analysis tools such as FreeSurfer (Fischl, 2012) have been used extensively in the scientific literature to analyze structural MRI examinations in order to extract region-specific biomarkers from brain examinations of healthy subjects and subjects with various neurological conditions, such as autism, multiple sclerosis, Alzheimer's disease, and schizophrenia (Salat et al., 2011; Kong et al., 2012; Deppe et al., 2014; Levman et al., 2017, 2018). Automated analysis tools have also been used to detect cortical thickness changes in adult MMD patients (Qiao et al., 2017, Lee et al., 2018).

Extensive research including pathological, genetic, and angiography studies have been carried out to understand the etiology of, and neurological changes caused by MMD. Recent studies have reported reduced cortical thicknesses in MMD patients (Qiao et al., 2017). In this study, we used T1-weighted MR images to assess regional abnormalities in the white matter (WM), grey matter (GM), the contrast of white matter to grey matter, and the relative regional volumes of white matter to grey matter in 269 examinations from patients with MMD by comparing them to the measurements from 993 MRI examinations from neurotypical control participants. Since regional GM and WM are directly connected with each other, biomarker metrics that combine measurements from two directly connected regions may provide more specific assessments of abnormalities that are based on a combination of irregular growth patterns in both GM and WM, particularly if the abnormal growth patterns affect GM and WM differently. Since there is a tendency for multiple structural T1 acquisitions to produce similar contrast between grey and white matter (these tissues have a common appearance across T1 pulse sequences), it was hypothesized that

regional relative signal intensities, which focus on the ratio of the white matter signal intensity to the grey matter signal intensity, may provide a degree of standardization for the comparison of signal intensity based biomarkers across pulse sequences. We hypothesize that thorough assessment of a large clinical population of MRI examinations will contribute to the body of data acquired on pediatric MMD and thus improve our collective understanding of the clinical presentation of the condition, which has been shown to exhibit regional abnormal growth in both the WM and GM (Kazumata et al., 2015; Qiao et al., 2020). We also hypothesize that relative regional volumes (RRVs) and signal intensities (RRSIs) may help better characterize the changes in the brains of patients with MMD and may represent biomarkers with the potential to assist in the assessment and characterization of brain development while potentially playing a role in overcoming varying protocol standardization challenges from clinical MRI examinations.

Materials and Methods

Participants

This study involved data from Boston Children's Hospital (BCH)'s clinical imaging database, which was retrospectively reviewed from January 1, 2008, to February 24, 2016, after ethics approval by the Institutional Review Board at BCH. Examinations of low quality (i.e. motion artefacts, metal artefacts from dental fixtures, and lack of volumetric structural T1-weighted examinations) were excluded from this study. Furthermore, examinations that were unavailable because of technical reasons were also excluded from the study. Neurotypical control participants were identified retrospectively in a previous study (Levman et al., 2017) as having a normal MRI examination assessment by a BCH neuroradiologist. Participants with an indication in their medical records of neurological problems including but not limited to autism, cerebral palsy, traumatic brain injury, developmental delay, multiple sclerosis, tuberous sclerosis complex, stroke, neurofibromatosis, cortical dysplasia, epilepsy, and attention deficit hyperactivity disorder, were excluded from the neurotypical cohort of this study. To avoid anomalous growth patterns affected by radiation treatments, patients diagnosed with any form of cancer were also excluded from the neurotypical control group. Patients with MMD were identified by the indication of moyamoya in their electronic patient medical record. This resulted in 993 healthy examinations and 269 MMD examinations, which were included for further analysis. The participant's age at the time of the examinations ranged between 0 and 38 years for the moyamoya population and between 0 and 31 years for the control group. The sex demographic and age distribution of the included participants is provided in the histogram in Figure 1.

MRI Data Acquisition and Preprocessing

This study involved the use of T1-weighted structural volumetric examinations obtained from patients imaged with 3 Tesla MRI scanners (Skyra, Siemens Medical Systems, Erlangen, Germany) at BCH. The retrospective nature of this study led to variability in the pulse sequences used to attain these T1-weighted structural volumetric images, which included numerous MPRAGE acquisitions, some traditional T1-weighted structural sequences, and volumetric spoiled gradient recalled sequences. There was variation in

spatial resolution, ranging from 0.2 to 1.4 mm. Examinations were excluded if patient motion artifacts were observed based on manual visual inspection. FreeSurfer's recon-all command (Fischl, 2012) was used to process the T1-weighted structural examinations, aligning each image to the available atlases. The following atlases were further considered for the extraction of volumetric and signal intensity (SI) measurements for the white and grey matter regions from each image: lh.aparc, rh.aparc, lh.w-g.pct, rh.w-g.pct, wmparc, and aseg. Thus, only the volumetric and mean signal intensity (SI) measurements were processed and analysed. The resultant data consisted of 36 white matter and 36 grey matter regions of interest in each hemisphere and one total brain WM and GM volume measurement. A description of all the regions of interest (ROI) investigated is summarized in Table 1. Regional relative signal intensity (RRSIs) and volumetric (RRVs) ratios were computed such that the extracted white matter measurement from each sub-region of interest was divided by the corresponding grey matter measurement for that same sub-region. This yielded a total of 143 ratios out of which 71 were extracted from the left hemisphere, 71 were extracted from the right hemisphere, and 1 ratio measurement represented the total white matter volume to total grey matter volume ratio calculated across the entire brain. It should also be noted that measurements for ROIs *lh/rhCorticalWhiteMatter, lh/rhCortex, CorticalWhiteMatter, and Cortex* only included volumetric information. Software that computes these regionally relative biomarkers from FreeSurfer version 6.0 output has been made available publicly to support future analyses (Ijner, 2021), and was implemented in the computer programming language python.

Statistical Analysis

The distribution of each ratio measurement from the healthy population was compared to the MMD population to help characterize regional abnormalities and differences in growth trajectories. Statistical analysis was performed to analyze the group-wise differences observable between the MMD population and neurotypical controls for the 143 ratios generated. This consisted of ratios of volumetric measurements, and signal intensity ratios from 993 exams from healthy subjects (controls) and 269 exams from subjects with MMD. Age bins of 5 years were used to divide participants into age groups of 0-5 years, 5-10 years, 10-15 years, and 15-20 years, representing early childhood, late childhood, early adolescence, and late adolescence, respectively. Our data for control participants consisted of only 27 subjects above the age of 20, which were ignored for the analysis in this study because of the small sample size, however, scatter plots include all age ranges for ease of visual comparison.

In order to test for group-wise differences between the FreeSurfer derived ratio measurements included in this analysis, a receiver operating characteristic curve (ROC) analysis was performed (Youngstrom, 2014). This produces the area under the ROC curve (AUC), a statistic which indicates higher group-wise separation as the AUC approaches 1. Cohen's *d* statistic was also computed for all ratios, which indicates a high degree of overlap (very similar distributions) between the two groups (MMD and Healthy) with a value close to 0 and positive/negative values indicate increased/decreased observed measurements in the MMD group. A standardized *t*-test (Student, 1908) was performed on each ratio measurement for the two groups to obtain a *p*-value. A Bonferroni corrected statistical

significance threshold was used to compensate for multiple statistical testing. The total number of ratio measurements compared for each age group was 143, yielding a threshold for statistical significance of $p < 0.05/143 = 3.49e^{-4}$. The ratio measurements were sorted in terms of diagnostic potential (in decreasing AUC order) and the leading measurements were visually assessed. All statistical analyses were performed with Matlab R2019a (Natick, MA, USA).

Results

Various regions of the brain demonstrate Bonferroni corrected statistically significant differences in white matter to grey matter ratios of volumetric measurements between patients with MMD and controls (Table 3). There are also a few regions that exhibit differences in the ratio of the mean signal intensities from the white and grey matter. Table 3 is sorted in decreasing order of the maximum AUC. The AUCs with corresponding p values not less than the determined Bonferroni corrected statistical threshold were not considered in this analysis. Table 3 also contains the d statistic value for all the age groups under each region. Of the 72 regions analyzed, 11 demonstrated group wise differences.

Differences in ratios of volumetric measurements is the highest in the insular region for the 15-20 year age group. Overall, the regions showing greatest differences in the ratios between the volumetric measurements are present on the lateral surface of the brain and show increased separation between the two groups at a higher age. The regions just above the corpus callosum on the medial surface of the brain, namely the posterior cingulate, caudal anterior cingulate, and isthmus cingulate demonstrated the greatest mean signal intensity (SI) ratio separation. The AUC values of the WM and GM measurements considered individually were also calculated and compared to the AUC obtained by computing their ratios (Table 4), for ease of assessment of the apparent utility of the proposed ratios (RRSIs and RRVs) as biomarkers relevant to MMD. Overall, there is often an increase in the AUC by relying on the RRSI and RRV ratios compared to the raw WM and GM measurements.

The ratio measurements for the leading AUC values were illustrated on scatterplots for visual assessment. The blue circles represent the computed ratios for neurotypical control subjects and the red circles represent the ratio for MMD patients. A rolling average was generated for the plots to visualize the difference in growth trends between the two groups. Figure 2 illustrates the scatter plots for the leading four regions from Table 3. The plots were generated for both hemispheres, however only the hemisphere with greater AUC have been included below due to relatively small differences between the two sides.

Discussion

In this study, we investigated the potential of regionally distributed relative volumes and regionally distributed relative signal intensities in assisting in characterizing MMD. This analytic approach helped identify a variety of brain regions exhibiting abnormal presentation in terms of the ratio of regional white matter to grey matter volumes (such as the insula, the lateral orbitofrontal region, etc.), as well as abnormal presentation of the ratio of regional white matter to grey matter signal intensities (such as the posterior cingulate, the

caudal anterior cingulate, etc.). Abnormal presentation of the insula confirms previously reported findings of insular abnormalities observed from functional MRI (fMRI) (Kazumata et al., 2017). Abnormal presentation of the lateral orbitofrontal region is supportive of previously reported findings identifying unique characteristics of the temporo-orbito frontal leptomeningeal network in pediatric MMD (Baltsavias et al., 2015). Abnormalities of the anterior cingulate and the insula identified in our study are in agreement with fMRI findings of reduced connectivity between the insula and the anterior cingulate (Kazumata et al., 2017). The agreements found between our primary findings and those in the literature potentially imply that RRSIs and RRVs may have utility in characterizing MMD, and may help standardize SI based analyses across pulse sequences.

It is unclear why the presentation of moyamoya disease differs by onset age. MMD exhibits a bimodal occurrence pattern, with common age of onset at both 5 and 40 years old (Baba et al., 2008; Miao et al., 2010; Ahn et al., 2014). In pediatric MMD, ischemic symptoms, seizures, and involuntary movements are common (Kim et al., 2010), while intracranial hemorrhage was observed in half of adults with MMD (Kuroda et al., 2008). A previous neuroimaging study on adult MMD demonstrated abnormal cortical thickness in the posterior cingulate, insula, precentral gyri, and postcentral gyri (Qiang et al., 2017). An additional previous neuroimaging study on pediatric MMD demonstrated abnormal cortical thickness in the insula, postcentral, precuneus and cingulate regions (Tompkins et al., 2021). We observed regional abnormal relative cortical volumes in the posterior cingulate, insula, pericalcarine gyri, transverse temporal, and superior temporal gyri. Although we could not compare pediatric MMD with adult onset MMD directly, there appears to be dominance of temporo-occipital lobe abnormalities in pediatric MMD and fronto-parietal lobe abnormalities in adult MMD, as well as insular and posterior cingulate abnormalities in both. A more detailed investigation would be required to reveal the correlation between distributions of abnormal cortical regions and cognitive functions.

Limitations of the study include the fact that traditional signal intensity based biomarkers (regional average signal intensity, etc.) extracted by publicly available software (Fischl, 2012) are heavily dependent on the pulse sequence selected, so observations of group-wise differences presents an extra analytic challenge. Since there is a tendency for multiple structural T1 acquisitions to produce similar contrast between grey and white matter (these tissues have a common appearance across T1 pulse sequences), it was hypothesized that regional relative signal intensities, which focus on the ratio of the white matter signal intensity to the grey matter signal intensity, may provide a degree of standardization for the comparison of signal intensity based biomarkers across pulse sequences. Future work will investigate the potential of additional signal intensity (SI) measurements included as part of this analysis, such as the regional minimum, maximum, range and standard deviation of SIs. Since it is known that variable MRI pulse sequences contribute to variable assessments of brain volume estimation (Haller et al., 2016), future work will investigate the distributional and sample size requirements in order to observe known effects on multi-protocol clinical MRI datasets. Thus, future work will investigate the distribution of regional SI biomarkers across large datasets with a variety of different pulse sequences all being well represented in the dataset, a task that was not possible in the clinical MRI dataset used in this study. It should be noted, however, that previous work comparing this same neurotypical cohort

(Levman et al., 2017) to pathological populations, has been relied upon to produce study findings that have been independently confirmed on public datasets in autism (Levman et al., 2018, 2019a, 2021) and have major findings that match those in literature studies in Down Syndrome (Levman et al., 2019b; McCann *et al.*, 2021). These types of validation are not possible in moyamoya disease at this time, but we are hopeful that our study findings will be reproducible despite the variable MRI pulse sequences employed. An additional limitation of this study was that it was done retrospectively with limited additional clinical and comorbid information for each patient, thus the potential impact of comorbidities such as brain lesions, infarction, atrophy or hemorrhage is unknown. Thus, future work will involve investigation of moyamoya patients prospectively, inclusive of detailed patient interviews in the context of a large patient population, which was not possible in this study due to limitations in the amount of information available in the electronic patient medical records. Future work will also investigate the potential for normalizing regional biomarkers by baseline regions not typically affected in moyamoya disease, such as the cerebellum.

Supplementary Material

Refer to Web version on PubMed Central for supplementary material.

Acknowledgements:

This work was supported by the National Institutes of Health (grant numbers R01HD078561, R21MH118739, HD098606, R03NS091587) to ET; Natural Science and Engineering Research Council of Canada's Canada Research Chair grant (grant number 231266) to JL, a Canada Foundation for Innovation and Nova Scotia Research and Innovation Trust infrastructure grant (R0176004) to JL, a Natural Science and Engineering Research Council of Canada Discovery Grant (R0192004) to JL and a St. Francis Xavier University research startup grant to JL (grant number R0168020). JL is founder of *Time Will Tell Technologies, Inc.*, otherwise the authors have no conflict of interest to report.

Data availability statement

The data relied upon in this study is private data from Boston Children's Hospital.

References

Ahn IM, et al. , Incidence, prevalence, and survival of moyamoya disease in Korea: a nation-wide population based study. Stroke. 45(4):1090–5, 2014. [PubMed: 24595588]

Baba T, et al. , Novel epidemiological features of moyamoya disease. J Neurol Neurosurg Psychiatry. 79(8):900–4, 2008. [PubMed: 18077479]

Baltsavias G, et al. , The collateral circulation in pediatric moyamoya disease. Childs Nerv Syst. 31(3):389–98, 2015. [PubMed: 25378261]

Chaudhuri R, et al. , Adult Moyamoya Disease: An Unusual Cause of Stroke. British Medical Journal. 307(6908):852–854, 1993. [PubMed: 8401131]

Deppe M, Tabelow K, Krämer J, Tenberge J-G, Schiffler P, Bittner S, Schwindt W, Zipp F, Wiendl H, Meuth SG,Evidence for early, non-lesional cerebellar damage in patients with multiple sclerosis: DTI measures correlate with disability, atrophy, and disease duration. Mult Scler 22, 73–84, 2016. 10.1177/1352458515579439 [PubMed: 25921041]

Duan L, Bao X-Y, Yang W-Z, Shi W-C, Li D-S, Zhang Z-S, Zong R, Han C, Zhao F, Feng J, Moyamoya disease in China: its clinical features and outcomes. Stroke. 43:56–60, 2012. 10.1161/STROKEAHA.111.621300 [PubMed: 22020027]

Fischl B, FreeSurfer. NeuroImage., 62(2):774–781, 2012. 10.1016/j.neuroimage.2012.01.021 [PubMed: 22248573]

Ganesan V, Moyamoya. Journal of Pediatric Neurology. 8(1):93–95, 2010.

Haller S, et al. , Basic MR sequence parameters systematically bias automated brain volume estimation. Functional Neuroradiology. 58:1153–1160, 2016.

Ijner P, Brain-Fractions, 10.5281/zenodo.4481949, 2021.

Kainth D, et al. , Epidemiological and clinical features of moyamoya disease in the USA. Neuroepidemiology. 40(4):282–7, 2013. [PubMed: 23445954]

Kamada F, et al. , A genome-wide association study identifies RNF213 as the first Moyamoya disease gene. J Hum Genet. 56(1):34–40, 2011. [PubMed: 21048783]

Kazumata K, et al. , Chronic ischemia alters brain microstructural integrity and cognitive performance in adult moyamoya disease. Stroke 46(2):354–360, 2015. [PubMed: 25538200]

Kazumata K, et al. , Mapping altered brain connectivity and its clinical associations in adult moyamoya disease: A resting-state functional MRI study. PLoS One 12(8):e0182759, 2017. [PubMed: 28783763]

Kim S-K, et al. , Pediatric moyamoya disease: an analysis of 410 consecutive cases. Ann Neurol. 68(1):92–101, 2010. [PubMed: 20582955]

Kim Y, et al. , High resolution MRI differences between moyamoya disease and intracranial atherosclerosis. European Journal of Neurology. 20(9):1311–1318, 2013. [PubMed: 23789981]

Kong L, Herold C, Stieltjes B, Essig M, Seidl U, Wolf RC, Wüstenberg T, Lässer MM, Schmid LA, Schnell K, Hirjak D, Thomann PA, Reduced Gray to White Matter Tissue Intensity Contrast in Schizophrenia. PLOS ONE 7:e37016, 2012. 10.1371/journal.pone.0037016 [PubMed: 22615876]

Kuroda S, Houkin K, Moyamoya disease: current concepts and future perspectives. Lancet Neurol. 7(11):1056–66, 2008. [PubMed: 18940695]

Lee J, et al. , Hemodynamic Impairment Measured by Positron-Emission Tomography Is Regionally Associated with Decreased Cortical Thickness in Moyamoya Phenomenon. Am J Neuroradiol 39(11):2037–2044, 2018. [PubMed: 30361434]

Levman J, MacDonald P, Lim AR, Forgeron C, Takahashi E, A pediatric structural MRI analysis of healthy brain development from newborns to young adults. Human Brain Mapping 38:5931–5942, 2017. 10.1002/hbm.23799 [PubMed: 28898497]

Levman J, Vasung L, MacDonald P, Rowley S, Stewart N, Lim A, Ewenson B, Galaburda A, Takahashi E, Regional volumetric abnormalities in pediatric autism revealed by structural magnetic resonance imaging. International Journal of Developmental Neuroscience 71:34–45, 2018. 10.1016/j.ijdevneu.2018.08.001 [PubMed: 30110650]

Levman J, MacDonald P, Rowley S, Stewart N, Lim A, Ewenson B, Galaburda A, Takahashi E, Structural Magnetic Resonance Imaging Demonstrates Abnormal Regionally-Differential Cortical Thickness Variability in Autism: From Newborns to Adults. Frontiers in Human Neuroscience, 13:75, 2019a. [PubMed: 30930758]

Levman J, MacDonald A, Baumer N, MacDonald P, Stewart N, Lim A, Cogger L, Shiohama T, Takahashi E, Structural Magnetic Resonance Imaging Demonstrates Abnormal Cortical Thickness in Down Syndrome: Newborns to Young Adults, NeuroImage: Clinical, 23:101874, 2019b. [PubMed: 31176294]

Levman J, MacDonald P, Rowley S, Stewart N, Lim A, Ewenson B, Galaburda A, Takahashi E, Structural Magnetic Resonance Imaging Demonstrates Abnormal Regionally-Differential Cortical Thickness Variability in Autism: From Newborns to Adults. Chapter in book titled: Brain Health and Clinical Neuroscience Editor's Pick 2021 edited by Leonhard Schilbach, Published by Frontiers Media SA, Published in: Frontiers in Human Neuroscience. ISSN 1664-8714, ISBN 978-2-88971-162-8, DOI 10.3389/978-2-88971-162-8. Pages 29–41, 2021.

Liu W, et al. , Identification of RNF213 as a susceptibility gene for moyamoya disease and its possible role in vascular development. PLoS One. 6(7):e22542, 2011. [PubMed: 21799892]

Miao W, et al. , Epidemiological and clinical features of moyamoya disease in Nanjing, China. Clin Neurol Neurosurg 112(3):199–203, 2010. [PubMed: 20004511]

Mineharu Y, et al. , Inheritance pattern of familial moyamoya disease: autosomal dominant mode and genomic imprinting. J Neurol Neurosurg Psychiatry. 77(9):1025–9, 2006. [PubMed: 16788009]

Papavasiliou A et al. , Familial Moyamoya disease in two European children. J Child Neurol. 22(12):1371–6, 2007. [PubMed: 18174554]

Qiao P-G, Zuo Z-W, Han C, Zhou J, Hong-Tao Z, Duan L, Qian T, Gong-Jie L, Cortical thickness changes in adult moyamoya disease assessed by structural magnetic resonance imaging. Clinical Imaging 46:71–77, 2017. [PubMed: 28734143]

Qiao P-G, et al. , MR Diffusional Kurtosis Imaging-Based Assessment of Brain Microstructural Changes in Patients with Moyamoya Disease before and after Revascularization. Am J Neuroradiol 41(2):246–254, 2020. [PubMed: 31974078]

Research Committee on the Pathology and Treatment of Spontaneous Occlusion of the Circle of Willis, et al. , Guidelines for diagnosis and treatment of moyamoya disease (spontaneous occlusion of the circle of Willis). Neurol Med Chir (Tokyo) 52(5):245–66, 2012. [PubMed: 22870528]

Salat DH, Williams VJ, Leritz EC, Schnyer DM, Rudolph JL, Lipsitz LA, McGlinchey RE, Milberg WP, Inter-individual variation in blood pressure is associated with regional white matter integrity in generally healthy older adults. NeuroImage 59(1):181–192, 2012. 10.1016/j.neuroimage.2011.07.033 [PubMed: 21820060]

Sawada T, Yamamoto A, Miki Y, Kikuta K, Okada T, Kanagaki M, Kasahara S, Miyamoto S, Takahashi JC, Fukuyama H, Togashi K, Diagnosis of moyamoya disease using 3-T MRI and MRA: value of cisternal moyamoya vessels. Neuroradiology 54:1089–1097, 2012. 10.1007/s00234-012-1020-1 [PubMed: 22349623]

Smith ER, Moyamoya Biomarkers. Journal of Korean Neurosurgical Society. 6(57):415–421, 2015.

Song P et al. , Magnetic Resonance Imaging (MRI) and Digital Subtraction Angiography Investigation of Childhood Moyamoya Disease. Journal of Child Neurology. 32(13), 2017.

Student, The Probable Error of a Mean. Biometrika 6:1–25, 1908. 10.2307/2331554

Suzuki J, Kodama N, Moyamoya disease--a review. Stroke 14:104–109, 1983. 10.1161/01.str.14.1.104 [PubMed: 6823678]

Tompkins G et al. , Cortical thickness in clinical moyamoya disease: A magnetic resonance imaging study. International Journal of Developmental Neuroscience, 2021. 10.1002/jdn.10146

Yamada I, Himeno Y, Suzuki S, Matsushima Y, Posterior circulation in moyamoya disease: angiographic study. Radiology 197:239–246, 1995. 10.1148/radiology.197.1.7568830 [PubMed: 7568830]

Yamada I, et al. , Moyamoya disease: diagnostic accuracy of MRI. Diagnostic Neuroradiology. 37:356–361, 1995b. [PubMed: 7477833]

Youngstrom EA, A Primer on Receiver Operating Characteristic Analysis and Diagnostic Efficiency Statistics for Pediatric Psychology: We Are Ready to ROC. J Pediatr Psychol 39:204–221, 2014. 10.1093/jpepsy/jst062 [PubMed: 23965298]

Zaharchuk G, Do Huy M, Marks Michael P, Rosenberg J, Moseley ME, Steinberg GK, Arterial Spin-Labeling MRI Can Identify the Presence and Intensity of Collateral Perfusion in Patients With Moyamoya Disease. Stroke 42:2485–2491, 2011. 10.1161/STROKEAHA.111.616466 [PubMed: 21799169]

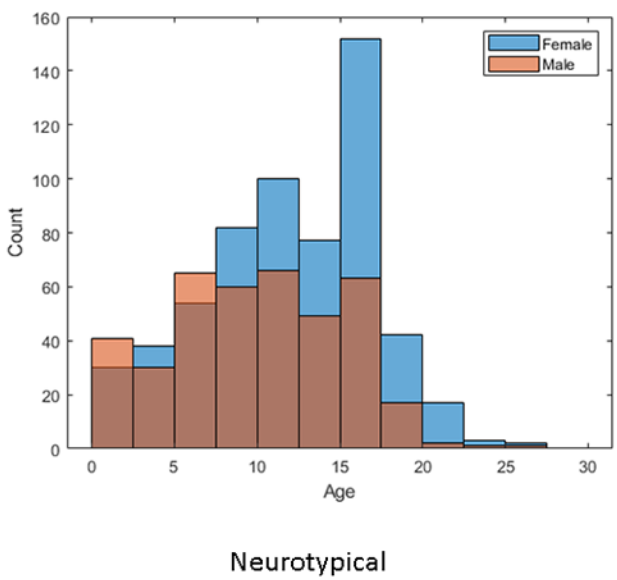

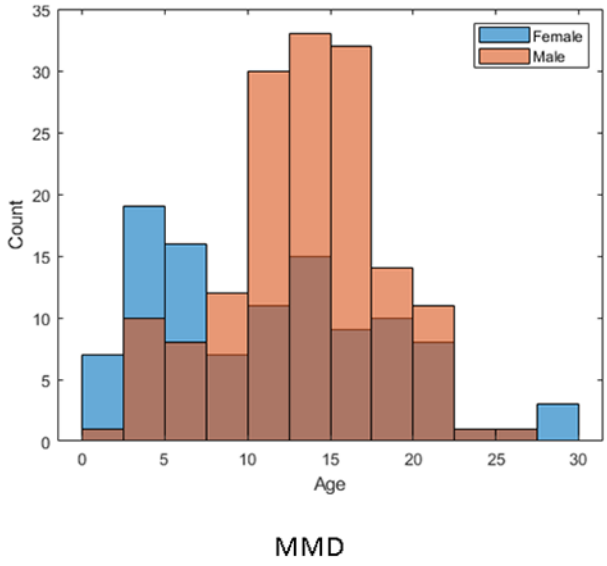

Figure 1.

Age distribution of all participants examined. Left: 993 healthy participants (593 females, 395 males). Right: 269 MMD patients (112 females, 157 males)

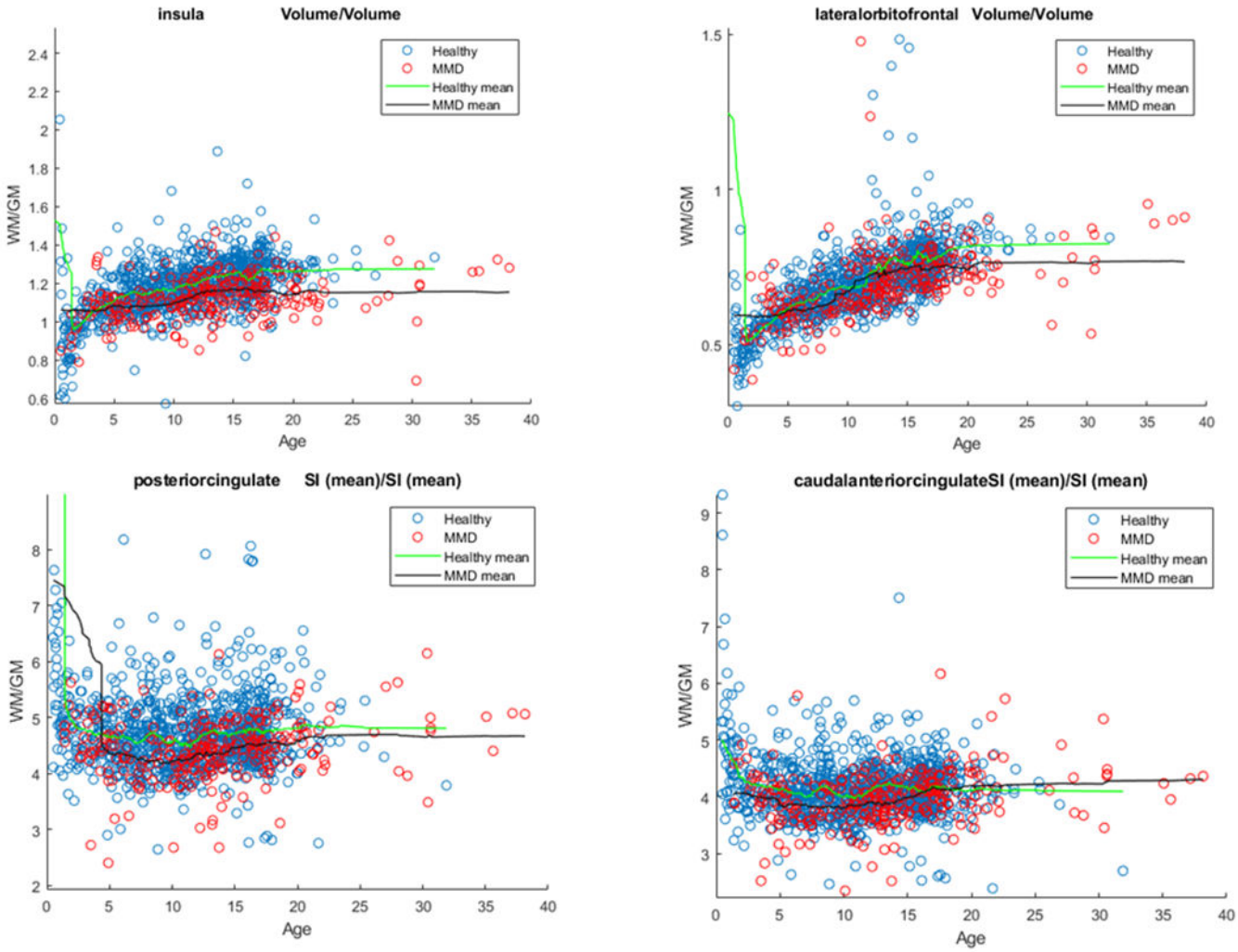

Figure 2.

Scatter plots illustrating differences in WM/GM volume and mean signal intensity ratios between healthy and moyamoya participants

Table 1

Measurements extracted for each region of interest using FreeSurfer

FreeSurfer ROI Label	Description	FreeSurfer ROI Label	Description
wm-lh-bankssts	left banks of superior temporal sulcus white matter	*ctx-lh-bankssts*	left banks of superior temporal sulcus grey matter
wm-lh-caudalanteriorcingulate	left caudal anterior cingulate white matter	*ctx-lh-caudalanteriorcingulate*	left caudal anterior cingulate grey matter
wm-lh-caudalmiddlefrontal	left caudal middle frontal white matter	*ctx-lh-caudalmiddlefrontal*	left caudal middle frontal grey matter
wm-lh-cuneus	left cuneus white matter	*ctx-lh-cuneus*	left cuneus grey matter
wm-lh-entorhinal	left entorhinal white matter	*ctx-lh-entorhinal*	left entorhinal grey matter
wm-lh-fusiform	left fusiform white matter	*ctx-lh-fusiform*	left fusiform grey matter
wm-lh-inferiorparietal	left inferior parietal white matter	*ctx-lh-inferiorparietal*	left inferior parietal grey matter
wm-lh-inferiortemporal	left inferior temporal white matter	*ctx-lh-inferiortemporal*	left inferior temporal grey matter
wm-lh-isthmuscingulate	left isthmus cingulate white matter	*ctx-lh-isthmuscingulate*	left isthmus cingulate grey matter
wm-lh-lateraloccipital	left lateral occipital white matter	*ctx-lh-lateraloccipital*	left lateral occipital grey matter
wm-lh-lateralorbitofrontal	left lateral orbitofrontal white matter	*ctx-lh-lateralorbitofrontal*	left lateral orbitofrontal grey matter
wm-lh-lingual	left lingual white matter	*ctx-lh-lingual*	left lingual grey matter
wm-lh-medialorbitofrontal	left medial orbitofrontal white matter	*ctx-lh-medialorbitofrontal*	left medial orbitofrontal grey matter
wm-lh-middletemporal	left middle temporal white matter	*ctx-lh-middletemporal*	left middle temporal grey matter
wm-lh-parahippocampal	left parahippocampal white matter	*ctx-lh-parahippocampal*	left parahippocampal grey matter
wm-lh-paracentral	left paracentral white matter	*ctx-lh-paracentral*	left paracentral grey matter
wm-lh-parsopercularis	left pars opercularis white matter	*ctx-lh-parsopercularis*	left pars opercularis grey matter
wm-lh-parsorbitalis	left pars orbitalis white matter	*ctx-lh-parsorbitalis*	left pars orbitalis grey matter
wm-lh-parstriangularis	left pars triangularis white matter	*ctx-lh-parstriangularis*	left pars triangularis grey matter
wm-lh-pericalcarine	left pericalcarine white matter	*ctx-lh-pericalcarine*	left pericalcarine grey matter
wm-lh-postcentral	left postcentral white matter	*ctx-lh-postcentral*	left postcentral grey matter
wm-lh-posteriorcingulate	left posterior cingulate white matter	*ctx-lh-posteriorcingulate*	left posterior cingulate grey matter
wm-lh-precentral	left precentral white matter	*ctx-lh-precentral*	left precentral grey matter
wm-lh-precuneus	left precuneus white matter	*ctx-lh-precuneus*	left precuneus grey matter
wm-lh-rostralanteriorcingulate	left rostral anterior cingulate white matter	*ctx-lh-rostralanteriorcingulate*	left rostral anterior cingulate grey matter
wm-lh-rostralmiddlefrontal	left rostral middle frontal white matter	*ctx-lh-rostralmiddlefrontal*	left rostral middle frontal grey matter
wm-lh-superiorfrontal	left superior frontal white matter	*ctx-lh-superiorfrontal*	left superior frontal grey matter

FreeSurfer ROI Label	Description	FreeSurfer ROI Label	Description
wm-lh-superiorparietal	left superior parietal white matter	*ctx-lh-superiorparietal*	left superior parietal grey matter
wm-lh-superiortemporal	left superior temporal white matter	*ctx-lh-superiortemporal*	left superior temporal grey matter
wm-lh-supramarginal	left supramarginal white matter	*ctx-lh-supramarginal*	left supramarginal grey matter
wm-lh-frontalpole	left frontal pole white matter	*ctx-lh-frontalpole*	left frontal pole grey matter
wm-lh-temporalpole	left temporal pole white matter	*ctx-lh-temporalpole*	left temporal pole grey matter
wm-lh-transversetemporal	left transverse temporal white matter	*ctx-lh-transversetemporal*	left transverse temporal grey matter
wm-lh-insula	left insula white matter	*ctx-lh-insula*	left insula grey matter
Left-Cerebellum-White-Matter	Left cerebellum white matter	*Left-Cerebellum-Cortex*	Left cerebellum grey matter
lhCorticalWhiteMatter	Left hemisphere cortical white matter	*lhCortex*	Left hemisphere cortical grey matter
wm-rh-bankssts	right banks of superior temporal sulcus white matter	*ctx-rh-bankssts*	right banks of superior temporal sulcus grey matter
wm-rh-caudalanteriorcingulate	right caudal anterior cingulate white matter	*ctx-rh-caudalanteriorcingulate*	right caudal anterior cingulate grey matter
wm-rh-caudalmiddlefrontal	right caudal middle frontal white matter	*ctx-rh-caudalmiddlefrontal*	right caudal middle frontal grey matter
wm-rh-cuneus	right cuneus white matter	*ctx-rh-cuneus*	right cuneus grey matter
wm-rh-entorhinal	right entorhinal white matter	*ctx-rh-entorhinal*	right entorhinal grey matter
wm-rh-fusiform	right fusiform white matter	*ctx-rh-fusiform*	right fusiform grey matter
wm-rh-inferiorparietal	right inferior parietal white matter	*ctx-rh-inferiorparietal*	right inferior parietal grey matter
wm-rh-inferiortemporal	right inferior temporal white matter	*ctx-rh-inferiortemporal*	right inferior temporal grey matter
wm-rh-isthmuscingulate	right isthmus cingulate white matter	*ctx-rh-isthmuscingulate*	right isthmus cingulate grey matter
wm-rh-lateraloccipital	right lateral occipital white matter	*ctx-rh-lateraloccipital*	right lateral occipital grey matter
wm-rh-lateralorbitofrontal	right lateral orbitofrontal white matter	*ctx-rh-lateralorbitofrontal*	right lateral orbitofrontal grey matter
wm-rh-lingual	right lingual white matter	*ctx-rh-lingual*	right lingual grey matter
wm-rh-medialorbitofrontal	right medial orbitofrontal white matter	*ctx-rh-medialorbitofrontal*	right medial orbitofrontal grey matter
wm-rh-middletemporal	right middle temporal white matter	*ctx-rh-middletemporal*	right middle temporal grey matter
wm-rh-parahippocampal	right parahippocampal white matter	*ctx-rh-parahippocampal*	right parahippocampal grey matter
wm-rh-paracentral	right paracentral white matter	*ctx-rh-paracentral*	right paracentral grey matter
wm-rh-parsopercularis	right pars opercularis white matter	*ctx-rh-parsopercularis*	right pars opercularis grey matter
wm-rh-parsorbitalis	right pars orbitalis white matter	*ctx-rh-parsorbitalis*	right pars orbitalis grey matter
wm-rh-parstriangularis	right pars triangularis white matter	*ctx-rh-parstriangularis*	right pars triangularis grey matter
wm-rh-pericalcarine	right pericalcarine white matter	*ctx-rh-pericalcarine*	right pericalcarine grey matter

FreeSurfer ROI Label	Description	FreeSurfer ROI Label	Description
wm-rh-postcentral	right postcentral white matter	*ctx-rh-postcentral*	right postcentral grey matter
wm-rh-posteriorcingulate	right posterior cingulate white matter	*ctx-rh-posteriorcingulate*	right posterior cingulate grey matter
wm-rh-precentral	right precentral white matter	*ctx-rh-precentral*	right precentral grey matter
wm-rh-precuneus	right precuneus white matter	*ctx-rh-precuneus*	right precuneus grey matter
wm-rh-rostralanteriorcingulate	right rostral anterior cingulate white matter	*ctx-rh-rostralanteriorcingulate*	right rostral anterior cingulate grey matter
wm-rh-rostralmiddlefrontal	right rostral middle frontal white matter	*ctx-rh-rostralmiddlefrontal*	right rostral middle frontal grey matter
wm-rh-superiorfrontal	right superior frontal white matter	*ctx-rh-superiorfrontal*	right superior frontal grey matter
wm-rh-superiorparietal	right superior parietal white matter	*ctx-rh-superiorparietal*	right superior parietal grey matter
wm-rh-superiortemporal	right superior temporal white matter	*ctx-rh-superiortemporal*	right superior temporal grey matter
wm-rh-supramarginal	right supramarginal white matter	*ctx-rh-supramarginal*	right supramarginal grey matter
wm-rh-frontalpole	right frontal pole white matter	*ctx-rh-frontalpole*	right frontal pole grey matter
wm-rh-temporalpole	right temporal pole white matter	*ctx-rh-temporalpole*	right temporal pole grey matter
wm-rh-transversetemporal	right transverse temporal white matter	*ctx-rh-transversetemporal*	right transverse temporal grey matter
wm-rh-insula	right insula white matter	*ctx-rh-insula*	right insula grey matter
Right-Cerebellum-White-Matter	Right cerebellum white matter	*Right-Cerebellum-Cortex*	Right cerebellum grey matter
rhCorticalWhiteMatter	Right hemisphere cortical white matter	*rhCortex*	Right hemisphere cortical grey matter
CorticalWhiteMatter	Total cortical white matter	*Cortex*	Total cortical grey matter

Table 2

Atlases used to extract volume and signal intensity measurements for the included regions from Table 1

Atlas	Measurements extracted for ROI	Hemisphere
wmparc	White matter - volume (mm3) - mean signal intensity (SI)	Left and right
lh.aparc *rh.aparc*	Grey matter - volume (mm3)	Left Right
lh.w-g.pct *rh.w-g.pct*	Grey matter - mean SI	Left Right
aseg	(For ROIs *Left/Right-Cerebellum-White-Matter, Left/Right-Cerebellum-Cortex, lh/rhCorticalWhiteMatter, lh/rhCortex, CorticalWhiteMatter, and Cortex*) White matter and grey matter - volume (mm3) - mean SI	Left and right

Table 3

Regions with greatest AUC values and Cohen's d statistic

Region name	Ratio type	MAX AUC	Ages 0-5 years L&R: AUC, d	Ages 5-10 years L&R: AUC, d	Ages 10-15 years L&R: AUC, d	Ages 15-20 years L&R: AUC, d
insula	Vol/Vol	0.7357664	L (0.41095, −0.080687) R (0.37838, −0.056888)	L (0.69233, −0.57897) R (0.60305, −0.34538)	L (0.68045, −0.63261) R (0.62333, −0.43904)	L (0.73577, −0.77011) R (0.708 , −0.8377)
lateralorbitofrontal	Vol/Vol	0.6716564	L (0.33589, −0.085619) R (0.32228, −0.079238)	L (0.67166, −0.58451) R (0.56188, −0.12163)	L (0.53265, −0.02372) R (0.56678, −0.1794)	L (0.61381, −0.2769) R (0.64719, −0.49359)
posteriorcingulate	SI (mean)/SI (mean)	0.6630753	L (0.63552, −0.06503) R (0.34668, 0.090706)	L (0.64818, −0.50465) R (0.63726, −0.49925)	L (0.66308, −0.58447) R (0.62912, −0.51332)	L (0.59871, −0.37084) R (0.5532 , −0.21278)
caudalanteriorcingulate	SI (mean)/SI (mean)	0.6574765	L (0.6839 , −0.35458) R (0.6501 , −0.52831)	L (0.64301, −0.21346) R (0.62947, −0.43064)	L (0.64757, −0.56645) R (0.65748, −0.5509)	L (0.63212, −0.44886) R (0.52956, −0.036785)
isthmuscingulate	SI (mean)/SI (mean)	0.6542827	L (0.57078, 0.095881) R (0.50486, −0.096746)	L (0.57449, −0.23401) R (0.4612 , 0.056035)	L (0.63316, −0.53216) R (0.65428, −0.55764)	L (0.50115, 0.027798) R (0.55533, −0.18207)
pericalcarine	Vol/Vol	0.6531284	L (0.38645, −0.012642) R (0.45246, −0.061226)	L (0.66667, −0.60478) R (0.59026, −0.28262)	L (0.65082, −0.52688) R (0.65313, −0.5088)	L (0.60705, −0.35263) R (0.62939, −0.48178)
transversetemporal	Vol/Vol	0.6507019	L (0.49232, −0.15733) R (0.39384, −0.0005625)	L (0.55573, 0.025443) R (0.51951, −0.10397)	L (0.57477, 0.2013) R (0.54077, 0.35746)	L (0.6507 , 0.5707) R (0.60219, 0.48277)
posteriorcingulate	Vol/Vol	0.6503963	L (0.48036, −0.11139) R (0.43078, −0.094991)	L (0.64141, −0.39961) R (0.68328, −0.57774)	L (0.54962, −0.20823) R (0.6504 , −0.51429)	L (0.62504, −0.41334) R (0.58125, −0.34424)
cuneus	SI (mean)/SI (mean)	0.6245575	L (0.63348, −0.1487) R (0.62843, −0.13824)	L (0.59913, −0.28476) R (0.45999, 0.048272)	L (0.62163, −0.50018) R (0.62456, −0.45696)	L (0.55095, −0.16811) R (0.52358, −0.081987)
superiortemporal	Vol/Vol	0.6129175	L (0.31587, −0.079959) R (0.28894, −0.068376)	L (0.58295, 0.28063) R (0.57324, 0.53345)	L (0.61292, 0.59564) R (0.58059, 0.45532)	L (0.58739, 0.32956) R (0.59753, 0.44694)
cerebellum	Vol/Vol	0.6063167	L (0.7274 , 0.48815) R (0.68277, 0.61321)	L (0.58741, 0.36016) R (0.53404, 0.51478)	L (0.50925, 0.005116) R (0.51685, 0.05507)	L (0.59147, 0.34623) R (0.60632, 0.52072)
frontalpole	Vol/Vol	0.6037156	L (0.24246, −0.0023755) R (0.2451 , −0.087736)	L (0.48721, 0.067726) R (0.60372, 0.59352)	L (0.56422, −0.19996) R (0.51533, 0.009963)	L (0.54391, −0.19555) R (0.58223, −0.18075)

Table 4

Comparison of AUC values for WM/GM ratio measurements to AUC of raw WM and GM measurements for regions in Table 3

Region name	Ratio type	Ages 0-5 years L&R: AUC (WM/GM, WM, GM)	Ages 5-10 years L&R: AUC (WM/GM, WM, GM)	Ages 10-15 years L&R: AUC (WM/GM, WM, GM)	Ages 15-20 years L&R: AUC (WM/GM, WM, GM)
insula	Vol/Vol	L (0.41095, 0.70309, 0.67577) R (0.37838, 0.6293, 0.60334)	L (0.69233, 0.58153, 0.51078) R (0.60305, 0.45527, 0.50931)	L (0.68045, 0.6134, 0.50058) R (0.62333, 0.58983, 0.49765)	L (0.73577, 0.57521, 0.53083) R (0.708, 0.53804, 0.58577)
lateralorbitofrontal	Vol/Vol	L (0.33589, 0.67752, 0.62658) R (0.32228, 0.64836, 0.591)	L (0.67166, 0.55284, 0.53782) R (0.56188, 0.47443, 0.58442)	L (0.53265, 0.53442, 0.53538) R (0.56678, 0.51329, 0.58531)	L (0.61381, 0.54326, 0.5151) R (0.64719, 0.5381, 0.53745)
posteriorcingulate	SI (mean)/SI (mean)	L (0.63552, 0.51322, 0.63659) R (0.34668, 0.58514, 0.61062)	L (0.64818, 0.55395, 0.63414) R (0.63726, 0.61234, 0.60126)	L (0.66308, 0.6336, 0.62032) R (0.62912, 0.50997, 0.54792)	L (0.59871, 0.53234, 0.55491) R (0.5532, 0.55269, 0.65069)
caudalanteriorcingulate	SI (mean)/SI (mean)	L (0.6839, 0.64992, 0.69301) R (0.6501, 0.54886, 0.66801)	L (0.64301, 0.51515, 0.63726) R (0.62947, 0.55284, 0.6153)	L (0.64757, 0.51895, 0.63193) R (0.65748, 0.57232, 0.62221)	L (0.63212, 0.53635, 0.59693) R (0.52956, 0.50312, 0.48641)
isthmuscingulate	SI (mean)/SI (mean)	L (0.57078, 0.56203, 0.55542) R (0.50486, 0.58672, 0.50214)	L (0.57449, 0.6083, 0.5515) R (0.4612, 0.55266, 0.46828)	L (0.63316, 0.60724, 0.60439) R (0.65428, 0.57948, 0.63308)	L (0.50115, 0.58717, 0.52378) R (0.55533, 0.52729, 0.54377)
pericalcarine	Vol/Vol	L (0.38645, 0.62989, 0.56903) R (0.45246, 0.57748, 0.26144)	L (0.66667, 0.5388, 0.56469) R (0.59026, 0.48534, −0.05049)	L (0.65082, 0.54487, 0.53771) R (0.65313, 0.55108, −0.24379)	L (0.60705, 0.51814, 0.60281) R (0.62939, 0.58506, −0.29193)
transversetemporal	Vol/Vol	L (0.49232, 0.57194, 0.55279) R (0.39384, 0.647, 0.56864)	L (0.55573, 0.49033, 0.53506) R (0.51951, 0.57783, 0.49884)	L (0.57477, 0.57813, 0.51997) R (0.54077, 0.56224, 0.49444)	L (0.6507, 0.5977, 0.56819) R (0.60219, 0.57033, 0.51679)
posteriorcingulate	Vol/Vol	L (0.48036, 0.73284, 0.70834) R (0.43078, 0.65263, 0.62998)	L (0.64141, 0.51132, 0.59766) R (0.68328, 0.62452, 0.70707)	L (0.54962, 0.51772, 0.54862) R (0.6504, 0.56353, 0.65355)	L (0.62504, 0.58251, 0.6612) R (0.58125, 0.62167, 0.65379)
cuneus	SI (mean)/SI (mean)	L (0.63348, 0.48571, 0.62911) R (0.62843, 0.52158, 0.61073)	L (0.59913, 0.61432, 0.63379) R (0.45999, 0.52343, 0.54816)	L (0.62163, 0.62413, 0.64151) R (0.62456, 0.56988, 0.63273)	L (0.55095, 0.67844, 0.57586) R (0.52358, 0.63577, 0.524)
superiortemporal	Vol/Vol	L (0.31587, 0.73702, 0.63475) R (0.28894, 0.66673, 0.57019)	L (0.58295, 0.54197, 0.51283) R (0.57324, 0.53662, 0.45224)	L (0.61292, 0.59589, 0.50233) R (0.58059, 0.57005, 0.48049)	L (0.58739, 0.54009, 0.53316) R (0.59753, 0.54624, 0.49427)
cerebellum	Vol/Vol	L (0.7274, 0.7029, 0.51653) R (0.68277, 0.68433, 0.55055)	L (0.58741, 0.52098, 0.58919) R (0.53404, 0.49554, 0.59204)	L (0.50925, 0.52692, 0.54743) R (0.51685, 0.5273, 0.54541)	L (0.59147, 0.53706, 0.53902) R (0.60632, 0.56628, 0.52333)
frontalpole	Vol/Vol	L (0.24246, 0.61212, 0.63768) R (0.2451, 0.6602, 0.57554)	L (0.48721, 0.55587, 0.55003) R (0.60372, 0.56848, 0.50882)	L (0.56422, 0.57394, 0.49263) R (0.51533, 0.56039, 0.57336)	L (0.54391, 0.49009, 0.53608) R (0.58223, 0.57184, 0.49408)